Laser-driven electron transfer through metal-insulator-metal contacts: Time-dependent configuration interaction singles calculations for a jellium model

Tillmann Klamroth*
Universität Potsdam, Institut für Chemie, Theoretische Chemie, Karl-Liebknecht Str. 24-25, D-14476 Golm, Germany
(Received 28 May 2003; revised manuscript received 2 September 2003; published 31 December 2003)

In this paper we report time-dependent configuration interaction singles calculations modeling the laser-induced current through a metal-insulator-metal (MIM) contact. We compare our results to recent experiments [D. Diesing, M. Merschdorf, A. Thon, and W. Pfeiffer, Appl. Phys. B (to be published)]. We use two jellium slabs separated by a vacuum region in a one-dimensional model to describe the MIM contact. The contact is coupled to ultrashort (fs) laser pulses by the semiclassical dipole approximation. We discuss simulated two-pulse correlation spectra in comparison to experimental results.

DOI: 10.1103/PhysRevB.68.245421 PACS number(s): 73.40.Gk, 72.10.−d

I. INTRODUCTION

Nanoscale contacts are very important for the ongoing miniaturization of electronic devices.[1,2] Especially interesting is the electron dynamics and thus charge transfer upon optical excitations in such nanoscale contacts for the fabrication of photoswitchable devices.

In this paper we simulate recent time-resolved photocurrent experiments in metal-insulator-metal contacts.[3] In these experiments an Al-Al_2O_3-Ag contact on a ZnSe substrate[4] is illuminated by two fs laser pulses from the Ag side of the contact with a photon energy of 1.5 eV and a variable delay time between the two pulses. The laser excitation leads to a photocurrent from the silver side of the contact through the insulating layer to the aluminum side. This reflects the fact that 80% of the laser energy is absorbed in the silver slab. Information about the excited electron dynamics and their lifetimes in the silver slab is obtained by measuring the photoinduced current as a function of the delay time between the two laser pulses. The experimental finding is that the laser-induced current through the metal-insulator-metal (MIM) contact is due to a mixture of two- and three-photon excitations of electrons on the silver side of the MIM contact, which are then injected as hot electrons into the aluminum side. From tunneling spectroscopy the barrier for the silver aluminum oxide interface is known to be 3.9 eV,[5] which is considerably more than twice the photon energy of 1.5 eV. Therefore, the two different processes are identified as internal photoemission for the three-photon process and tunneling of excited electrons through the insulating barrier for the two-photon process, respectively. Due to electron-electron scattering the involved, intermediate-excited single-electron states in the silver layer are not stationary but have finite lifetimes in the order of femtoseconds, which is represented by a strong dependence of the photocurrent on the delay time between the two laser pulses.

These experimental findings have consequences for a theoretical simulation which will be discussed in the following. Kinetic models for electron excitation and deexcitation in metals like the two-temperature model[6] cannot be used here, since no electron temperature can be assumed and coherence effects are important for the investigated time scales. For the same reason time-independent Landauer theory for electron transport[7] is not applicable. Many theoretical descriptions of excited electron dynamics at metal interfaces have been carried out using a one-electron picture. For example, the decay of negative ion resonances on clean (e.g., Refs. 8 and 9) and adsorbate covered surfaces (e.g., Ref. 10) have been successfully modeled. But since the many-electron dynamics, especially the electron-electron scattering in the silver layer after laser excitation, is the most important process leading to the observed photocurrent, one cannot use a one-electron picture for a theoretical description of such a system. Therefore, a level of theory has to be used which somehow accounts for the electron-electron scattering. Also electron correlation effects might be quite important for describing these processes. So for the theory one faces the challenge of simulating the electron dynamics for a system with a practically infinite number of degrees of freedom. Hence, the two choices one has are either to treat the whole system approximately with as many degrees of freedom as possible or to use a so-called system bath approach, where the total Hamiltonian is split into a small system part treated usually on a high level of theory and a heat bath coupled to it. One example for the latter one is the so-called open-system density matrix approach, which, for example, has been applied to the dynamics of image potential states at metal surfaces.[11] We believe that an approximate treatment of the whole system is favorable here, because the division of the total Hamiltonian into a system part and a bath part seems to be quite problematic for the description of the dynamics of metal electrons.

An exact solution of the time-dependent Schrödinger equation is only feasible for very few electrons and therefore for small molecules like H_2.[12] Most commonly used for the simulation of many-electron dynamics are the time-dependent density functional theory[13] (TDDFT), and the time-dependent Hartree-Fock method (TDHF), which was first introduced for atom-ion collisions[14] and later for ionization processes.[15] TDDFT approaches have been extensively applied among other systems to nonlinear electron dynamics in metal clusters.[16] Here, we want to use a different approach based on one of the simplest methods to recapture the electron-electron correlation for excited states, the so-called configuration interaction singles (CIS) method.[17] The CIS method is a widely used tool in molecular physics and quan-

tum chemistry for approximate calculations of excited states with singly excited Slater determinants starting from an uncorrelated restricted Hartree-Fock (HF) ground-state wave function. The general experience is that most excited states are described qualitatively correctly by this method. However, the method fails for states which have a dominant contribution of higher order—for example, doubly excited Slater determinants. This means we can only describe states which are formed mainly by one-electron excitations and thus only scattering events between one electron and another are included in such an approach. This would be problematic if one is interested in the details of the electron-electron scattering on the way to thermalization after excitation. But we think, for the charge transfer process under investigation, the important feature is the initial decay and/or dephasing of the single-electron excitation, which seems to be described qualitatively correctly in the present model as shown in the following. Since the proposed method is a closed quantum system model—i.e., an approximate solution of the time-dependent Schrödinger equation—it is anyway only suitable for short-time propagations, where short means before the first major recurrences of the wave function. On the other hand, as an advantage, no assumptions about lifetimes due to electron-electron scattering have to be made like in an open-system density matrix description.

In the experiments, MIM contacts consisting of a 15-nm Ag slab separated from a 30-nm Al slab by 2 nm of Al_2O_3 are used. Clearly such a device cannot be modeled in a purely *ab initio* fashion. Thus in our model calculations we restrict ourselves to a one-dimensional model, including only the z direction perpendicular to the metal-insulator-metal contact, which is also the direction of electron flow. Furthermore, we model the two metals by freestanding jellium slabs, separated by a 2-nm vacuum gap replacing the insulating layer. Although this is a quite simple model, we believe it is still interesting to investigate whether the basic experimental results can be reproduced in such fashion—e.g., whether an approximate closed-quantum-system model can be applied in such a situation. Unfortunately a qualitatively more realistic model from a microscopic point of view is numerically to demanding at the present time.

II. THEORETICAL MODEL

A. Hartree-Fock solution

The laser-driven electron dynamics will be expressed in the basis of the restricted Hartree-Fock ground-state Slater determinant of the static (field-free) MIM contact and singly excited determinants derived thereof. As a first step, we therefore need to solve the restricted Hartree-Fock equations

$$\hat{f}(z)\psi_i(z)=\varepsilon_i\psi_i(z). \tag{1}$$

Here $\psi_i(z)$ are the spatial canonical HF orbitals and ε_i the orbital energies. The first $N/2$ orbitals are occupied with two electrons of opposite spin, all other orbitals are virtual (unoccupied), with N being the total number of electrons. The Fock operator $\hat{f}(z)$ includes the kinetic energy of the electrons, the external potential (V_{ext}), and the electron-electron interaction ($\hat{V}_{ee}$):

$$\hat{f}(z)=-\frac{1}{2}\frac{d^2}{dz^2}+V_{ext}(z)+\hat{V}_{ee}. \tag{2}$$

Since we work in a one-dimensional model, the Coulomb interaction, contained in $V_{ext}(z)$ and $\hat{V}_{ee}$, is regularized in the following way;[18] for the latter, this means

$$\hat{V}_{ee}=\sum_{b=1}^{N/2}(2\hat{J}_b-\hat{K}_b), \tag{3}$$

$$\hat{J}_b\psi_i(z)=\int dz'\left[\psi_b^{\star}(z')\psi_b(z')\frac{1}{\sqrt{(z-z')^2+c}}\right]\psi_i(z), \tag{4}$$

$$\hat{K}_b\psi_i(z)=\int dz'\left[\psi_b^{\star}(z')\psi_i(z')\frac{1}{\sqrt{(z-z')^2+c}}\right]\psi_b(z). \tag{5}$$

The same is done for the external potential, which consists in our model of the attraction $V_{ek}(z)$, caused by the uniform positive-charge background $\rho^+(Z)$ for both jellium slabs, and a harmonic confinement in both outer vacuum regions $V_b(z)$, which is added to prevent the electrons from reaching the grid edge in the time-dependent calculations:

$$V_{ext}(z)=V_{ek}(z)+V_b(z), \tag{6}$$

with

$$V_{ek}(z)=-\int\frac{\rho^+(Z)}{\sqrt{(z-Z)^2+c}}dZ, \tag{7}$$

$$\rho^+(Z)=\begin{cases}\rho_{Al}^+, & Z_{Al,S_1}<Z<Z_{Al,S_2},\\ \rho_{Ag}^+, & Z_{Ag,S_1}<Z<Z_{Alg,S_2},\\ 0, & \text{otherwise},\end{cases} \tag{8}$$

and

$$V_b(z)=\begin{cases}k[z-(Z_{Al,1_2}-z_b)]^2, & z<Z_{Al,1_2}-z_b,\\ k[z-(Z_{Alg,S_2}+z_b)]^2, & z>Z_{Alg,S_2}+z_b,\\ 0, & \text{otherwise}.\end{cases} \tag{9}$$

Here c is chosen to be $1a_o^2$, $k=0.000\,012E_h/a_0^2$, and $z_b=155a_0$. Sometimes the parameter c is used to fit computed values to experimental data such as work functions. However, since c has no strict physical meaning, we prefer to keep it fixed and use ρ_{Al}^+ and ρ_{Ag}^+ for fitting (see below). The thicknesses of the aluminum and silver layer are $Z_{Al,S_2}-Z_{Al,S_1}$ and $Z_{Ag,S_2}-Z_{Ag,S_1}$ and are chosen according to the experiments[3] as 29.8 nm and 15.3 nm, respectively; see Fig. 1.

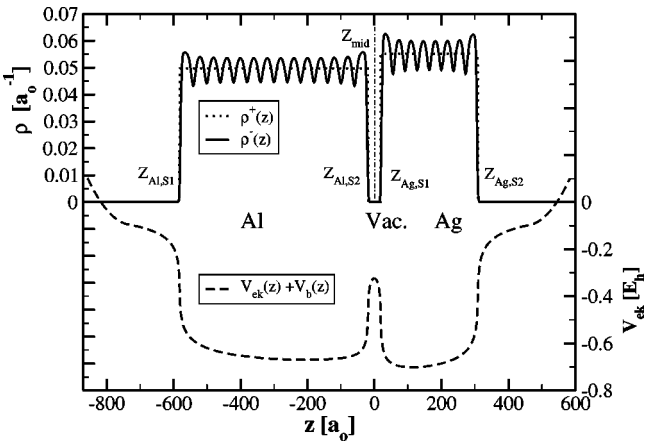

FIG. 1. Shown are the positive-charge background $\rho^+(z)$ for both jellium slabs (dotted line), the resulting attractive potential $V_{ek}(z)$ with the harmonic confinement $V_b(z)$ added (dashed line), and the resulting HF ground-state electron density $\rho^-(z)$ for the model system used. On the left is the Al slab, on the right the Ag slab, and in between 2 nm ($37.8a_0$) of vacuum.

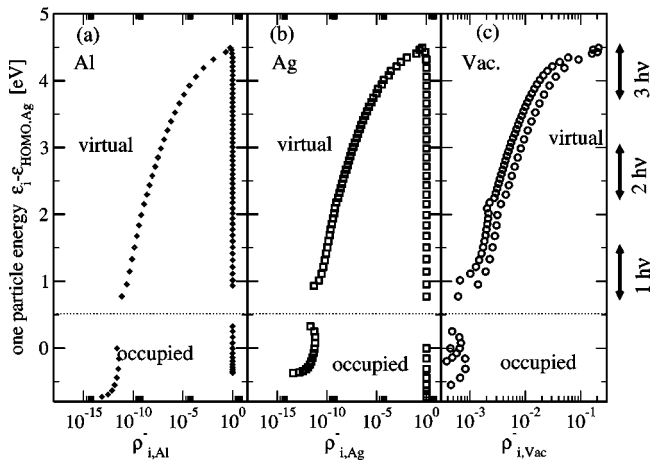

FIG. 2. Shown is the partial norm on the Al side, $\rho^-_{i,Al}$ (a), and on the Ag side, $\rho^-_{i,Ag}$ (b), of those canonical HF orbitals, 22 occupied and 76 virtual orbitals, which are mainly located in the MIM contact, as a function of the HF orbital energy relative to the energy of the highest occupied orbital on the Ag side. It is $\rho^-_{i,Al}=1-\rho^-_{i,Ag}$. (c) shows the partial norm inside the barrier region. The arrows on the right indicate the energy ranges for one-, two-, and three-photon excitations of single electrons from occupied silver orbitals, which cover an energy range of ≈ 0.73 eV.

The remaining parameters ρ^+_{Al} and ρ^+_{Ag} are formally the jellium background densities of Al and Ag and are chosen in such a way that the energy of the highest occupied canonical HF orbital for the isolated metal slabs is in the range of the work functions of Al and Ag. Since not much is known about the crystallographic lattice orientation of the metal slabs in the contact experimentally, we only consider roughly the range of possible work functions for typical Al and Ag surfaces. Typical work functions for aluminum are $\Phi_{Al}(100)=4.41$ eV, $\Phi_{Al}(110)=4.06$ eV, and $\Phi_{Al}(111)=4.24$ eV.[19,20] For silver the work functions are a bit larger, $\Phi_{Ag}(100)=4.64$ eV, $\Phi_{Ag}(110)=4.52$ eV, and $\Phi_{Ag}(111)=4.74$ eV.[21,22] Furthermore, we demand the integrated value for ρ^+ to be an even number, since we use a restricted HF formalism. We take ρ^+_{Al} as 0.049 $73e/a_o$ and ρ^+_{Ag} as 0.055 $19e/a_o$. By this choice, our model consists of 28 electrons in the Al slab and 16 in the Ag slab. The energies of the highest occupied HF orbital are -4.54 eV (Ag) and -4.22 eV (Al) for the isolated slabs.

The molecular orbitals (MO's) are calculated by a damped self-consistent-field (SCF) scheme, where the Fourier grid method[23–25] is applied for the kinetic energy of the electrons. We use a grid basis with 1300 points and a grid spacing of 1.108 $34a_0$ to represent the MO's in the RHF calculation. This means that we include about $274a_0$ of vacuum on both outer sides of the jellium slabs in our model. Figure 1 shows the resulting $\rho^+(Z)$ and $\rho^-(z)=\Sigma_i^{N/2}2|\psi_i(z)|^2$ for our model system. We obtain one-particle energies ε_i for the occupied orbitals ranging from $-0.1807E_h$ to $-0.1551E_h$ for the orbitals located on the left side (Al) and from $-0.1938E_h$ to $-0.1671E_h$ for the ones on the right side (Ag).

Particularly interesting is the nature of the canonical HF orbitals for our model system—i.e., how localized they are in the silver and aluminum slabs or in the insulating layer. As we want to express the many-electron dynamics in the basis of singly excited Slater determinants, we have to ensure that our basis provides suitable orbitals for the processes we want to model: namely, hot electron tunneling and internal photoemission. Therefore, we computed the partial norm of the orbitals left and right from the midpoint of the vacuum slab, $z_{mid}=0$, $\rho^-_{i,Al}/\rho^-_{i,Ag}$, and the partial norm inside the barrier region between Z_{Al,S_2} and Z_{Ag,S_1}, $\rho^-_{i,vac,}$ as

$$\rho^-_{i,Al}=\int_{-\infty}^{z_{mid}}|\psi_i(z)|^2dz, \tag{10}$$

$$\rho^-_{i,Ag}=\int_{z_{mid}}^{\infty}|\psi_i(z)|^2dz, \tag{11}$$

$$\rho^-_{i,vac}=\int_{Z_{Al,S_2}}^{Z_{Ag,S_1}}|\psi_i(z)|^2dz. \tag{12}$$

Note that these three numbers do not add up to 1 because the norm inside the barrier region is counted twice. The results for all those orbitals, 22 occupied and the first 76 virtual orbitals, which are mainly located in the MIM contact—i.e., which are approximately zero in the outer vacuum region—are shown in Fig. 2 as a function of the one-particle energies relative to the highest occupied silver orbital. The arrows on the right indicate the energy range of single-electron excitations from occupied silver orbitals by 1, 2 and 3 times the photon energy of 1.5 eV. These occupied silver orbitals cover an energy range of ≈ 0.73 eV, which is also the arrow length. As one can see in Figs. 2(a) and 2(b), the one-photon excitation leads to orbitals which have only a negligible probability (in the order 10^{-10}) on the opposite side of the contact. For the two-photon excitation the orbitals are still very localized to one or the other side, but they have a much increased partial norm inside the barrier, which makes them

suitable as initial states for excited electron tunneling. In the three-photon region around 4 eV the characteristics of the virtual orbitals change dramatically. They become substantially delocalized and have a large probability to be inside the barrier. This indicates that an excitation to these orbitals would result in internal photoemission and corresponds nicely to the experimental band offset for the silver aluminum oxide interface of 3.9 eV.[5] Also one can see a considerable gap in the orbital energies between the highest occupied orbital and the first virtual orbital. This is a well-known problem of the HF theory for metallic systems—i.e., the vanishing density of states around the Fermi level. However, as discussed above, the processes investigated here take place far away from the Fermi energy and the expected effect of this shortcoming on the results is very small.

B. CIS states

We use the configuration interaction singles method to calculate excited many-electron wave functions and energies. The wave function is expanded in singly excited Slater determinants, where one electron is promoted from an occupied orbital a to a virtual orbital b starting from the HF ground state Slater determinant. We only include singlet configuration state functions (CSF's) in our expansion,[26] since we are interested in optical transitions and no spin-orbit coupling is included in our Hamiltonian. The CIS states are thus

$$\Psi_{CIS,i}=C_{0,i}\Psi_0+\sum_{a\in occ}\sum_{b\in virt}C_{ai}^{b}\,{}^1\Psi_a^b. \tag{13}$$

Here, Ψ_0 is the HF ground-state wave function and ${}^1\Psi_a^b$ is a linear combination of excitations of the α spin electron from the spatial orbital a to b (Ψ_a^b) and the β spin electron ($\Psi_{\bar{a}}^{\bar{b}}$) forming a singlet:

$${}^1\Psi_a^b=\frac{1}{\sqrt{2}}(\Psi_a^b-\Psi_{\bar{a}}^{\bar{b}}). \tag{14}$$

The Hamiltonian matrix elements in this basis are as follows:[17]

$$\langle\Psi_0|\hat{H}_0-E_{HF}|{}^1\Psi_a^b\rangle=0,$$

$$\langle{}^1\Psi_a^b|\hat{H}_0-E_{HF}|{}^1\Psi_c^d\rangle=(\varepsilon_b-\varepsilon_a)\delta_{ac}\delta_{bd}-\langle\ ab|cd\ \rangle+2\langle\ ac|bd\ \rangle, \tag{15}$$

with the system Hamiltonian

$$\hat{H}_o=V_{ek}-\frac{1}{2}\sum_i\frac{d^2}{dz_i^2}+\sum_i\sum_{j>i}\frac{1}{\sqrt{(z_i-z_j)^2+c}}. \tag{16}$$

We get excitation energies and the excited-state wave functions by diagonalizing this Hamilton matrix:

$$\mathbf{H}_0\vec{C}_i=E_i\vec{C}_i. \tag{17}$$

The occupied and all virtual orbitals with an energy less than $0.051E_h$ are included in the expansion. Altogether, the 22 occupied and 148 virtual spatial orbitals, which are used for excitation, result in a total of 3257 CSF's and thus in 3257 states. The excited-state energies relative to the HF ground-state energies obtained by the CIS calculations are in a range from 0.15 to 6.6 eV. A larger calculation with 199 virtual orbitals gives only a maximal change of 0.015 eV for important excitation energies up to 4.5 eV.

C. Time propagation

The time-dependent Schrödinger equation is solved in order to describe the laser-induced electron dynamics. We use the semiclassical dipole approximation to couple the system to the laser pulses:

$$i\dot{\Psi}(t)=\hat{H}(t)\Psi(t), \tag{18}$$

with

$$\hat{H}(t)=\hat{H}_0-\hat{\mu}F(t,z), \tag{19}$$

where $\hat{\mu}=ez$ is the dipole operator and $F(t,z)$ the electric field due to the two pulses:

$$F(t,z)=f(z)\{F_{0,1}(t)\cos[\omega_p(t-t_{p,1})]+F_{0,2}(t)\cos[\omega_p(t-t_{p,2})]\}. \tag{20}$$

The single-pulse envelopes are chosen as $\cos^2$ functions:

$$F_{0,i}=F_{max}\cos^2\left[\frac{\pi}{2\sigma_p}(t-t_{p,i})\right], \tag{21}$$

where F_{max} is the maximum field strength and σ_p the pulse width for both pulses. $t_{p,i}$ $(i=1,2)$ is the time where the first and second pulses are maximal, respectively. These pulses may be delayed by a time $\Delta\tau$—i.e., $t_{p,2}=t_{p,1}+\Delta\tau$. Like in the experiments, $\hbar\omega_p$ is 1.5 eV and $\sigma_p=20$ fs. $f(z)$ includes a z dependence in the electric field to account for the experimental situation, where the laser pulse hits the contact from the silver side and about 80% of the pulse energy is absorbed before reaching the insulator layer. The explicit form of $f(z)$ is chosen as

$$f(z)=\begin{cases}1, & z>Z_{Ag,S2},\\ \exp[-\beta(Z_{Ag,S2}-z)], & Z_{Ag,S1}<z<Z_{Ag,S2},\\ 0.11, & Z_{Al,S2}<z<Z_{Ag,S1},\\ 0.079\exp[-\lambda(Z_{Al,S2}-z)], & Z_{Al,S1}<z<Z_{Al,S2},\\ 0.01, & z<Z_{Al,S1},\end{cases} \tag{22}$$

with $\beta=0.002\ 33a_0^{-1}$ and $\lambda=0.003\ 34a_0^{-1}$, based on the experimental findings given in Ref. 5

The time-dependent electronic wave function is expanded in the basis of the CIS states as

$$\Psi(t)=\sum_i D_i(t)\Psi_{CIS,i}, \tag{23}$$

and the initial wave function is the HF ground-state wave function Ψ_0. The time propagation is done using a split op-

erator technique[27] during those periods when the first and/or second pulse are ''on.'' The wave function at time $t+\Delta t$ is computed from the wave function at time t as

$$|\Psi(t+\Delta t)\rangle = \{\exp(-i\hat{H}_0\Delta t/2)\mathbf{U}^\dagger \times \exp[-iF(t)\bar{\mu}\Delta t]\mathbf{U} \times \exp(-i\hat{H}_0\Delta t/2)\}|\Psi(t)\rangle. \quad (24)$$

Here, $\mathbf{U}$ is the transformation matrix, which transforms from the eigenfunctions of $\hat{H}_0$ to those of $\hat{\mu}f(z)$. Further, $\bar{\mu}$ is the diagonal dipole operator in its eigenfunction space. The possible time step Δt depends strongly on the maximal field strength F_{max} and varies between 0.05 and 0.01 fs in the calculations shown here.

After the time $t_1 = \max(t_{p,1}, t_{p,2}) + \sigma_p$, when two pulses are over, the wave function can be propagated with arbitrary time steps since $\hat{H}_0$ is diagonal in the field-free eigenstate basis:

$$\Psi(t_2) = \exp[-i\hat{H}_0(t_2-t_1)]\Psi(t_1) = \sum_i D_i(t_1)\exp[-iE_i(t_2-t_1)], \quad (25)$$

where E_i is the energy of the i th CIS state.

D. Calculation of laser-induced charge transfer

The reduced one-electron density matrix $\rho(z',z;t)$ is computed out of the time-dependent wave function in order to calculate the charge transfer from Ag to Al during the propagation:

$$\rho(z',z;t) = N \int \int \cdots \int \Psi(z',z_2,\cdots,z_N,\omega_1,\cdots,\omega_N;t)^\star \times \Psi(z,z_2,\cdots,z_N,\omega_1,\cdots,\omega_N;t) \times dz_2,\cdots,dz_N d\omega_1,\cdots,d\omega_N. \quad (26)$$

Here z_i are the spatial coordinates and ω_i the spin coordinates of the electrons. The electron density $\rho(z;t)$ is represented by the diagonal elements of $\rho(z',z;t)$. The charge transfer from Ag to Al is

$$\mathrm{CT}_{\mathrm{Al}\leftarrow\mathrm{Ag}}(t) = \int_{-\infty}^{z_{mid}} [\rho(z;t)-\rho(z;t_0)]dz, \quad (27)$$

where $z_{mid}=0$ is the midpoint of the vacuum slab.

III. RESULTS

A. Results for $\Delta\tau = 0$

Figure 3 shows the time-dependent charge transfer $\mathrm{CT}_{\mathrm{Al}\leftarrow\mathrm{Ag}}(t)$ from Ag to Al for zero delay time between pulses 1 and 2 for $F_{max}=4\times10^7$ V/m, which is the experimental field strength. One can see that the main charge transfer occurs during the time of the laser pulse and shortly afterwards. The end of the pulse is indicated by the vertical dotted line. A couple of fs after this time the amount of charge transfer is more or less oscillating around a certain value. These oscillations represent back and forth charge transfer processes, which, however, are much smaller than the initial charge transfer. Therefore, most of the initially transferred charge density is trapped on the Al side during the investigated time scales due to scattering with other electrons on the Al side of the contact.

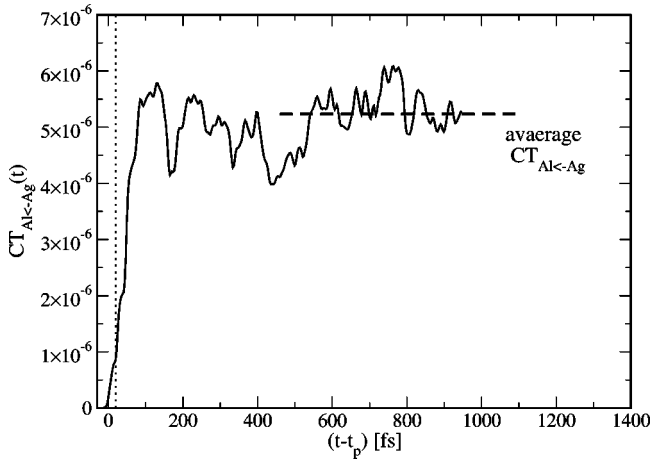

FIG. 3. The time-dependent charge transfer from Ag to Al $\mathrm{CT}_{\mathrm{Al}\leftarrow\mathrm{Ag}}(t)$ (see text) for zero delay time between the two laser pulses for $F_{max}=4\times10^7$ V/m. The end of the pulse is indicated by the vertical dotted line, the computed average charge transfer from Ag to Al $\overline{\mathrm{CT}}_{\mathrm{Al}\leftarrow\mathrm{Ag}}$ by the dashed line.

The current through the contact is the time derivative of $\mathrm{CT}_{\mathrm{Al}\leftarrow\mathrm{Ag}}(t)$ as shown in Fig. 3. Because of the highly oscillatory behavior of $\mathrm{CT}_{\mathrm{Al}\leftarrow\mathrm{Ag}}(t)$, however, this is not a very practical measure for the laser-induced current. Since in the experiments only time-averaged currents are measured,[3] we compute the average charge transfer from Ag to Al, $\overline{\mathrm{CT}}_{\mathrm{Al}\leftarrow\mathrm{Ag}}$ and take this to be proportional to the laser-induced current. The average $\overline{\mathrm{CT}}_{\mathrm{Al}\leftarrow\mathrm{Ag}}$ is calculated by averaging $\mathrm{CT}_{\mathrm{Al}\leftarrow\mathrm{Ag}}(t)$ over the time interval between 460 fs and 945 fs after the maximum of the first pulse. This time interval is, on the one hand, beginning sufficiently late after the second pulse for the delay times investigated (up to 100 fs); on the other hand, we see no major change of $\mathrm{CT}_{\mathrm{Al}\leftarrow\mathrm{Ag}}(t)$ on this time scale. This shows that there is indeed no major recurrence of the wave function as it was directly after the pulse and thus the time interval is short enough to be used in this closed-quantum-system model. Extending the propagation time further would be unphysical anyway, because then the energy transfer due to electron phonon coupling should become important, which is left out completely in our model calculations.

In Fig. 4 the averaged charge transfer $\overline{\mathrm{CT}}_{\mathrm{Al}\leftarrow\mathrm{Ag}}$ for different F_{max} and for the zero delay time is shown. Up to $F_{max}=1\times10^7$ V/m the charge transfer is proportional to F_{max}^2, which indicates by arguments from time-dependent perturbation theory a one-photon process. Nevertheless, the amount of transferred charge is very small for this field strength. Then the slope becomes steeper and steeper, ending in a mixture of a $\sim F_{max}^4$ behavior (two-photon process) and a $\sim F_{max}^6$ behavior (three-photon process) for field strengths

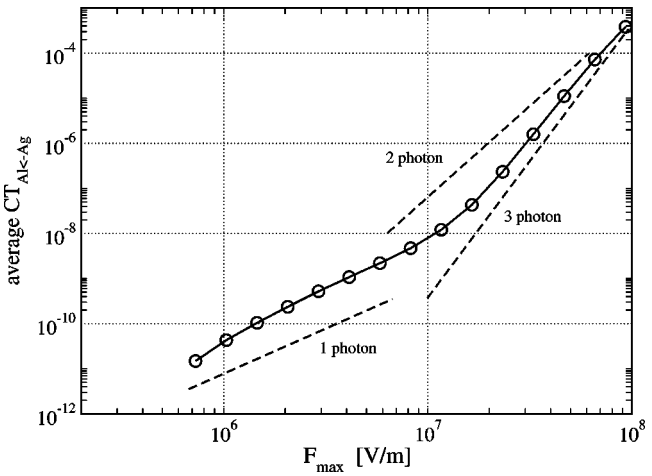

FIG. 4. The average charge transfer from Ag to Al $\overline{\mathrm{CT}}_{\mathrm{Al}\leftarrow\mathrm{Ag}}$ (see text) as a function of F_{max} for zero delay time between the two laser pulses. The dashed lines indicate the slopes one would expect for an ideal one-, two-, or three-photon process.

larger than 2×10^7 V/m. This indicates that the charge transfer in this region is mainly caused by a mixture of two- and three-photon processes as in the experiment, where the applied field strength was 4×10^7 V/m.

B. Two-pulse correlation

The experimental two-pulse correlation spectra from Ref. 3 is shown in Fig. 5 (b) together with the simulated ones (a). The photoinduced current and the simulated average charge transfer, respectively, are displayed as a function of the delay time between the two pulses and the frequency components of the signals are shown. The spectrum in (a) is calculated with the experimental field strength of 4×10^7 V/m. The experimental spectrum is normalized to the signal at a delay of 150 fs, the simulated one to twice the average charge transfer of a single pulse.

One sees a large current for zero delay time between both laser pulses in the experimental spectrum. This current is about 20 times the current for the nonoverlapping pulses. For a pure two-photon process one would expect the current for $\Delta\tau=0$ to be 8 times $[\sim(2\ F_{max})^4]$ larger than the one for two isolated pulses $[\sim 2\ F_{max}^4]$. For a pure three-photon process the current at zero delay time should be 32 times the one for isolated pulses $[\sim(2\ F_{max})^6$ vs$\sim 2\ F_{max}^6]$. Therefore, one concludes that the laser assisted current is due to a mixture of two- and three-photon processes at $F_{max}=4\times10^7$ V/m. This is confirmed by the frequency components of the spectrum. There one sees a pronounced peak at 2 and 3 times the photon frequency. After a delay time of about 50 fs all structure is lost in the experimental spectrum and the signal is nearly constant. This means that by this time most of the information about the first laser pulse is lost in the system. One would say in a single-electron picture that most of the electrons excited by the first laser pulse have relaxed back to lower-lying states after this time. One can expect the electron-electron scattering to be the dominant process on such a short time scale, while electron-phonon coupling should be not so important.

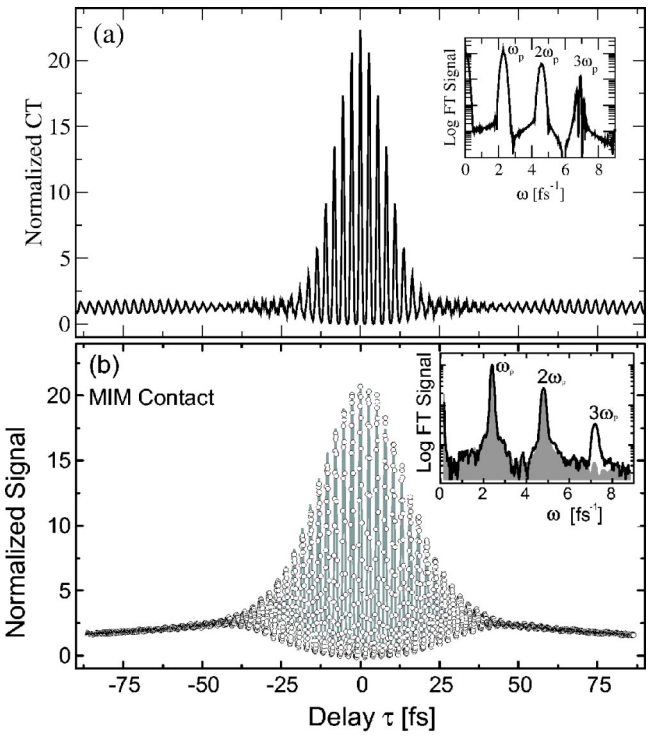

FIG. 5. **(b)** The experimental laser assisted current form Ag to Al depending on the delay time between the two laser pulses and its frequency components (Ref. 3). (a) The same for the calculated average charge transfer for the experimental field strength of $F_{max}=4\times10^7$ V/m. The experimental spectrum is normalized to the signal at a delay of 150 fs, the simulated one to twice the average charge transfer of a single pulse.

The calculated spectrum in Fig. 5(a) has the same overall structure as the experimental one. It shows a slightly larger enhancement of about 22 for zero delay time. The calculated charge transfer is also caused by a mixture of a two- and a three-photon excitation. This can be seen even more clearly by comparing the frequency components of the calculated and the experimental spectrum, which are in good agreement. Therefore, the simulation successfully reproduces the basic charge transfer mechanisms. Like the experimental spectrum, the calculated one shows no major signal recurrences for delay times up to about 75 fs as shown in the graph. Nevertheless, it still has some structure for long delay times compared with the experiment, because only 16 silver electrons are included in our model. Also the simulated signal is smaller around zero delay times. This is caused to a large part by the fact that for computational convenience we have chosen $\cos^2$ pulses instead of more realistic Gaussian pulses. Apart from this, we find that already this few electrons account for a large part of the electron-electron scattering for delay times up to 30 fs, as the time scale of the first drop in the signal envelope is quite well reproduced by our simulations. Therefore, the loss of coherence in the signal can be simulated for short delay times with a closed-quantum-system model. Nevertheless, one has to keep in mind that in the present calculations this is only due to internal redistribution of energy and phase and in a closed

quantum system information about the first pulse will never be lost. For the same reason we believe one should be cautious in attributing this apparent loss of coherence to population transfer or dephasing, which are only rigorously defined in the framework of an open-quantum-system model.

IV. CONCLUSIONS

We computed CIS excited-state wave functions for a one-dimensional jellium model of a (Al-Al_2O_3-Ag) MIM contact starting from a canonical restricted Hartree-Fock ground-state wave function. We performed simulations of the laser-driven many-electron dynamics in the basis of the CIS wave functions. In general agreement between theory and experiment has been achieved, regarding the two spectra shown in Fig. 5. The overall structure and therefore the time scale of electron-electron scattering are comparable. Also, the two different contributions to the charge transfer from Ag to Al are well reproduced. We believe that the method used is quite promising for simulating short-time-scale many-electron dynamics. For smaller systems the method could be used for more realistic, three-dimensional external potentials and/or higher-order excitations, which will lead to a much better agreement with experiments. Unfortunately this is beyond the scope of currently available computer power for the nanoscale MIM contacts considered here. We plan to apply it to smaller systems, where, we believe, the use of CIS or higher-order CI wave functions computed by *ab initio* quantum chemistry programs could lead to much improved accuracy of the theoretically calculated electron dynamics.

ACKNOWLEDGMENTS

We thank Walter Pfeiffer and Peter Saalfrank for fruitful discussions. This work has been supported by the Deutsche Forschungsgemeinschaft (Grant No. SPP-1093, Project No. Sa 547/5).

*Electronic address: klamroth@rz.uni-potsdam.de

[1] *Molecular Electronics*, edited by J. Jortner and M. Ratner (Blackwell, Oxford, 1997).
[2] A. Nitzan, Annu. Rev. Phys. Chem. **52**, 681 (2001).
[3] D. Diesing, M. Merschdorf, A. Thon, and W. Pfeiffer, J. Appl. Phys. B (to be published).
[4] D. Diesing, A. W. Hassel, and M. M. Lohrengel, Thin Solid Films **342**, 282 (1999).
[5] A. Thon, Ph.D. thesis, Julius-Maximilians-Universität, Würzburg, 2002.
[6] S. I. Anisimov, B. L. Kapeliovich, and T. L. Perel'man, Sov. Phys. JETP **39**, 375 (1974).
[7] S. Datta, *Electronic Transport in Mesoscopic Systems* (Cambridge University Press, Cambdirge, England, 1995).
[8] J. P. Gauyacq, A. G. Borisov, and G. Raşeev, Surf. Sci. **490**, 99 (2001).
[9] A. G. Borisov, J. P. Gauyacq, and S. V. Shabanov, Surf. Sci. **487**, 243 (2001).
[10] J. Sjakste, A. G. Borisov, and J. P. Gauyacq, Nucl. Instrum. Methods Phys. Res. B **203**, 49 (2003).
[11] T. Klamroth, P. Saalfrank, and U. Höfer, Phys. Rev. B **64**, 035420 (2001).
[12] K. Harumiya, I. Kawata, H. Kono, and Y. Fujimura, J. Chem. Phys. **113**, 8953 (2000).
[13] E. Runge and E. K. U. Gross, Phys. Rev. Lett. **52**, 997 (1984).
[14] K. C. Kulander, K. R. S. Devi, and S. E. Koonin, Phys. Rev. A **25**, 2968 (1982).
[15] K. C. Kulander, Phys. Rev. A **36**, 2726 (1987).
[16] F. Calvayrac, P.-G. Reinhard, E. Suraud, and C. A. Ullrich, Phys. Rep. **337**, 493 (2000).
[17] J. B. Foresman, M. Head-Gordon, J. A. Pople, and M. J. Frisch, J. Phys. Chem. **96**, 135 (1992).
[18] R. Grobe and J. H. Eberly, Phys. Rev. A **48**, 4664 (1993).
[19] J. K. Grepstad, P. O. Gartland, and B. J. Slagsvold, Surf. Sci. **57**, 348 (1976).
[20] R. M. Eastment and C. H. B. Mee, J. Phys. F: Met. Phys. **3**, 1738 (1973).
[21] A. W. Dweydari and C. H. B. Mee, Phys. Status Solidi A **27**, 223 (1975).
[22] A. W. Dweydari and C. H. B. Mee, Phys. Status Solidi A **17**, 247 (1973).
[23] R. Kosloff, J. Phys. Chem. **92**, 2087 (1988).
[24] C. C. Martson and G. G. Balint-Kurti, J. Chem. Phys. **91**, 3571 (1989).
[25] D. T. Colbert and W. H. Miller, J. Chem. Phys. **96**, 1982 (1992).
[26] R. Paunz, *Spin Eigenfunctions* (Plenum, New York, 1979).
[27] A. D. Bandrauk, E. Aubanel, and S. Chelkowski, *Femtosecond Chemistry* (Verlag Chemie, 1995), Vol. 2, Chap. 25, p. 731.